Energetic and electronic properties of P Doping at the rutile TiO_2 (110) surface from first-principles

Run Long, Niall J. English

The SEC Strategic Research Cluster and the Centre for Synthesis and Chemical Biology, Conway Institute of Biomolecular and Biomedical Research, School of Chemical and Bioprocess Engineering, University College Dublin, Belfield, Dublin 4, Ireland.

Abstract: The energetic and electronic properties of various P doping configurations at the rutile TiO_2 (110) surface are investigated by first-principles density functional theory (DFT) calculations. Several substitution and adsorption configurations for P impurities at the surface and the subsurface are considered. The stability of the P-doped systems is compared on the basis of the calculated formation energy and adsorption energy. Our calculated results indicate that the P impurities replace surface Ti atoms preferentially under O-rich growth conditions , and surface O atoms under Ti-rich conditions. In addition, it was found that the creation of oxygen vacancies favors P incorporation at substitution sites but not at adsorption sites. Doping with a single P atom into an O site may lead to either anionic or cationic states in the dopant. This causes either band-to-band transitions or introduces gap states to band transitions, with the former corresponding to a small band gap narrowing or broadening and the latter resulting in obvious reductions of photon transition energy. Substitutional replacement of Ti atoms by P atoms and adsorption on the surface (P-cation doping)

results in either a small band reduction or a slight band gap enlargement, depending on the doping sites. It is speculated that the interaction between P impurities and surface oxygen vacancies will lead to further enhanced photocatalytic activity in the visible light region.

Keywords: rutile TiO_2 (110) surface, P doping, electronic structure

1. Introduction

TiO_2 has been widely used as a promising photocatalyst for water splitting and hydrogen production due to its high photocatalytic activity, resistance to photocorrosion, photostability, low cost and non-toxicity [1, 2]. Unfortunately, the range of optical absorption of TiO_2 is limited to the **ultraviolet** region due to its large band gap (3.0 eV for rutile and 3.2 eV for anatase), which occupies only about ~5% of the whole solar photon spectrum. In recent decades, anion doping of TiO_2 with nonmetal elements like nitrogen [3-5] and carbon [6, 7] has been investigated widely to narrow the band gap of TiO_2 and to shift the optical absorption edge to the visible-light region. **Doping with metal elements, such as Cr and Sb, has also received much attention [8, 9], which serves to reduce electron-hole recombination in the Cr-Sb codoped case or to create oxygen vacancies for Cr-doping.**

For cation-modified titania, doping with non-metal cation species has attracted considerable attention recently. Ohno et al. reported that S^{4+} were incorporated as

cations and replaced Ti^{4+} in S-doped TiO_2 [10, 11] and showed photocatalytic activity under visible light and stronger visible light absorption than N, C, and S anion-doped TiO_2. Yu et al. [12] synthesized S^{6+}-doped TiO_2, the band gap narrowing in which should be similar to conventional transition metal doping. Certainly, S can also be doped in an ionic state into TiO_2 to give photocatalytic activity under visible light irradiation [13]. Recently, Lin et al. reported that P-cation doped anatase TiO_2 nanoparticles had high photocatalytic activity with respect to pure samples under visible light [14]. The impurity was shown to be in a pentavalent-oxidation state (P^{5+}) according to XPS and with the form of Ti-O-P as identified by FT-IR. They claimed further that the doped P^{5+} replaced part of Ti^{4+} rather than incorporation in the form of PO_4^{3-} in the anatase lattice [15]. On the other hand, Lin et al. reported that P-doped TiO_2 with P in a lower oxidation state narrowed the band gap by about 0.13 eV compared to pure TiO_2 and that the absorption tail is in visible light region [16]. However, Yu et al. reported that P-modified TiO_2 leads to a blue-shift due to enlargement by 0.07 eV of the band gap [17].

Since most of the photoreactivity properties of materials are related to surface processes, the analysis of doping at the surface is of great significance. It has been shown that surface defects play an important role in the chemistry of TiO_2 [18, 19]. Therefore, the surface characteristics of a photocatalyst should be closely related with its photocatalytic performance. In surface science, the rutile TiO_2 (110) surface has become the most studied oxide surface, and it generally used to model TiO_2 catalytic properties under ultrahigh vacuum conditions [20, 21]. Therefore, in this paper, we

present a systemic investigation on the energetic and electronic properties of P impurities incorporated by substitutional and adsorptive mechanisms into the rutile (110) surface.

To obtain a comprehensive understanding of P-doped rutile (110) surface, we performed DFT calculations to investigate the effects of P doping on the energetic and electronic structure. Various substitutional and adsorptive P configurations at the surface and the subsurface layers were considered. The stability of these different P doping models was compared according to their formation energies and adsorption energies. **The influence of P dopants on the electronic properties of P-doped rutile (110) surfaces is systemically discussed.** In addition, the interaction between P impurities and surface oxygen vacancies have a positive effect on photocatalytic activity under visible light , by consideration of their electronic structures. Our theoretical analysis provides a possible explanation for the modification of band gap reported by different experiments with P anion and cation doping [14-17].

2. Computational Details

All of the spin-polarized DFT calculations were performed using the projector augmented wave (PAW) pseudopotentials in the Vienna *ab initio* Simulation Package [22, 23] (VASP). The Perdew and Wang parametrization [24] of the generalized gradient approximation [25] was adopted for the exchange-correlation potential. The electron wave function was expanded in plane waves up to a cutoff energy 400 eV and a Monkhorst–Pack *k*-point mesh [26] of 4 × 4 × 1 was used for geometry

optimization and electronic property calculations. The cell and atomic relaxations were carried out until the residual forces were below 0.01 eV/Å. The optimized lattice parameters were found to be a = 4.608 Å and c = 2.956 Å for rutile, in good accord with experimental values and other theoretical calculated results [27, 28], indicating that our computational approach is reasonable.

The P-doped/adsorbed rutile (110) surface was modeled with a 60-atom (2 × 1) supercell composed of five TiO_2 layers. The side view and top view of this system are shown in Figures 1(a) and 1(b). The depth of the supercell was 30.53 Å, and the thickness of the vacuum layer above the slab was 15 Å. **Although this system has been used to model B-doped rutile (110) surfaces [29], we used a 120-atom (2 × 2) supercell to simulate both the pure state and one of the substitutional P-doped configurations (the O_s case mentioned in part 3.1, at half of the P concentration), to verify if the 2 × 1 supercell is sufficiently large to describe the P-doped systems. It was found that the bond lengths were essentially identical in the pure case, with a 4% difference for the P-doped case. The difference in the formation energy was less than 2%. Hence, the 2 × 1 supercell was judged to be** sufficiently large to lead to good convergence of energies and properties. The atoms in the bottom layer were fixed to their optimized bulk positions in order to simulate the presence of the bulk underneath. This configuration has been shown to minimize well-known energy oscillations as a function of the number of layers (even-odd) [30], and has proven to agree well with recent experimental studies [31]. The relaxed Ti-O bond lengths at or near the pure rutile TiO_2 surface are listed in Table 1 as well as

experimental data [31] and previous theoretical calculated results [32]. Table 1 shows that our calculated bond lengths are good agreement with previous theoretical and experimental values [31, 32]. This indicates that our model affords a reasonable description of the rutile TiO_2 (110) surface.

Substitutional P doping was carried out by replacement of one O or one Ti per supercell with one P atom, corresponding to 1.67% P concentration at the rutile (110) surface. **This approximates the P concentration used in various experiments, in the range of 1.2%~2% [14-17].** Adsorption of P was performed by addition of one P atom to the rutile TiO_2 (110) surface. As shown in part 3.1B, there are six different adsorption sites on the surface. The properties of a surface O vacancy were investigated by removal of one bridging O atom on the surface, either in the presence of substitutional or adsorptive P dopants. To compare the relative stability of the P-doped systems, the formation energies E_f of the substitutionally doped systems (for either O or Ti) were estimated according to

$$E_f = E(P-doped) - E(pure) - \mu_P + \mu_O \qquad (1)$$

$$E_f = E(P-doped) - E(pure) - \mu_P + \mu_{Ti} \qquad (2)$$

The following was used to calculated the adsorption energy E_{ad} for adsorptive doping

$$E_{ad} = E(P-doped) - E(pure) - \mu_P \qquad (3)$$

in which $E(P-doped)$ is the total energy of the supercell containing the P impurity, $E(pure)$ denotes the total energy with or without one bridging surface O vacancy, while μ_P, μ_O and μ_{Ti} represent the chemical potentials of the P, O, and Ti atoms, respectively. It should be noted that the formation energy depends on growth

conditions, which may be either O- or Ti-rich [33]. μ_O and μ_{Ti} obey the relationship $\mu_{Ti} + \mu_O = \mu(TiO_2)$. Under Ti-rich growth conditions, μ_{Ti} is assumed to be the energy of one atom in bulk Ti ($\mu_{Ti} = \mu_{Ti}^{metal}$) and μ_O was calculated by the above formula. Under O-rich growth conditions, μ_O was estimated from consideration of the O_2 molecule (*i.e.*, $\mu_O = \mu(O_2)/2$) and the chemical potential of Ti was taken again as that of one atom in bulk Ti. The chemical potential μ_P was calculated from the formula $\mu_P = \frac{1}{4}[(P_4O_{10}) - 5\mu(O_2)]$.

3. Results and Discussion

3.1 P Implantation on Rutile TiO_2 (110) Surface

In this section, our main concern is to establish whether substitution at the surface is favored with respect to the substitution in sub-layers. We consider two kinds of P doping, *i.e.*, anion- and cation-doping, with various possible non-equivalent surface and subsurface substitutional P atom arrangements. Substitution was limited to the first two layers in the slab. There are mainly five non-equivalent substitutional P to O arrangements, namely, bridging (O_b), sub-bridging (O_{sb}), sub-bridging-2 (O_{sb2}), surface (O_s) and subsurface (O_{ss}), which are shown in Figure 1 (a). There are two types of Ti atoms on the rutile TiO_2 (110) surface. One is the sixfold coordinated Ti between the two bridging O atoms and the other is a fivefold coordinated Ti in the subsurface. Thus, we consider four possible substitutional configurations, *i.e.*, Ti_{5c}, Ti_{6c}, Ti_{s6c}, and Ti_{s6c2}.

A. Substitutional P Doping

The formation energies of the different substitutionally doped systems are summarized in Table 2. It indicates that sites may be ordered based on thermodynamic favorability of adsorption: (1) for P anion doping, $O_s > O_{ss} > O_b > O_{sb} > O_{sb2}$; (2) for P cation doping, $Ti_{5c} > Ti_{6c} > Tis_{6c} > Ti_{s6c2}$. Further, the formation energy of Ti_{5c} is 2.15 eV (12.08 eV) but it is 14.37 eV (9.61 eV) for the O_s–doped configuration under O-rich growth conditions (the numbers in parenthesis in Table 2 represent the formation energies under Ti-rich growth conditions). This indicates that P occupies preferentially the surface fivefold coordinated Ti atom site (Ti_{5c}) under O-rich conditions. On the other hand, under Ti-rich growth conditions, substitution of the O atom at O_s site is energetically favorable. However, it should be noted that it still possesses a high formation energy of 9.61 eV. Hence, P-cation doping at the Ti_{5c} site is the preferred site in actual experiments due to the requirement of relatively small formation energies for energetic feasibility. The results indicate also that the P anion doping is preferential under Ti-rich growth conditions while P cation doping is preferential under O-rich conditions. Hence, our theoretical calculations indicate that the form of P ions (cation or anion) in P-doped TiO_2 depends on growth conditions. It should be noted that replacement of the O_{ss} site atom requires only about 0.01 eV more than the O atom at O_s site and the energy difference is only 0.09 eV between the Ti_{5c} and Ti_{6c}-substituted configurations. Therefore, we shall discuss details of the electronic properties of the four models O_s, O_{ss}, Ti_{5c} and Ti_{6c}.

To study the variation in the oxidization state of the P dopant, the total charge

densities of P-doped O_s, O_{ss},Ti_{5c} and Ti_{6c} were calculated and are shown in Figures 2 (a)-(d) (top panel). Figure 2(a) shows the contour plot of charge density near the surface of the O_s–substituted configuration, in which the P atom and adjacent Ti atoms form three strong P-Ti bonds (shown only in one plane consisting of two P-Ti bonds), implying a negative oxidization state. **Two P-Ti bonds are 2.443 Å in length, while the third P-Ti bond is 3.200 Å and is very weak; this induces significant structural distortion vis-à-vis the original O-Ti bonds (2.028 and 1.949 Å). There are two possible reasons responsible for this change. One arises from the larger atomic radius of the P relative to the O ion, and the other is the lower electronegativity of the B atom in comparison to the O atom, which leads to a decrease in electron cloud overlapping and weakens the strength of the P-Ti bond, as well as elongating the P-Ti bond length.** For the O_{ss}–substituted configuration (cf. Figure 2(b), however, only one P-Ti bond is formed, and two P-O bonds are formed between P and the two O atoms which are under the P-Ti plane. **The P-Ti bond length is 2.401 Å and the two P-O bond lengths are 2.718 Å; the P-Ti bond is elongated substantially vis-à-vis the original O-Ti bonds (1.972 Å), indicating a relatively small interaction between P and Ti.** It appears that the larger radius of P atom vis-à-vis the O atom (0.98 vs 0.48 Å) [34] leads to a large local distortion. Calculation of the Bader charge for this P dopant confirmed its cationic state. For the Ti_{5c}–substituted case, Figure 2(c) shows that the P atom and adjacent oxygen atoms form five P-O bonds (shown in one plane), indicating a positive oxidation state for P. **Four of these P-O bond lengths are 1.719 Å while one is 1.604**

Å in length. These have contracted with respect to the original O-Ti bond lengths (1.949 and 1.838 Å), indicating that interaction between P and O is strong. It is possible that this may be attributed to different ionic radii between P and Ti ions. For the Ti_{6c} case (cf. Figure 2(c)), six P-O bonds are formed (shown in one plane) between the P atom and adjacent O atoms, suggesting that P may exist as a cation. **The calculated P-O bond lengths are 1.682, 1.706, and 1.970 Å, respectively, indicating contraction in comparison to the original Ti-O bond lengths (1.848, 2.104, and 2.028 Å). Similarly to the case of Ti_{5c} model, the smaller P ion radius than that of the Ti ion is responsible for the contraction in bond length.** To investigate this further, we calculated the Bader charge [35, 36] of the P atom in O_s, O_{ss}, Ti_{5c}, and Ti_{6c}-substituted cases, and found the corresponding Bader charges on the P atom to be -0.74 e, 1.43 e, 0.56 e, and 5.0 e anionic and cationic P-doping configurations, respectively. Hence, the form of the P dopant in doped titania materials may be either anionic or cationic, depending on the synthesis method and experimental conditions, and such variation has been noted by various experimental studies [14-17].

To investigate the effects of P substitution on electronic structure and photocatalytic activity, the density of states (DOS) and projected density of states (PDOS) of both O_s- and O_{ss}-substituted systems and Ti_{5c}- and Ti_{6c}- doped systems were calculated and are shown in Figures 3 and 4, respectively. For comparison, the DOS and PDOS of undoped rutile TiO_2 (110) surfaces are shown also.

For substitutional P to -O doping, there is an obvious difference in the electronic

structure between the O_s and O_{ss} cases. For the O_s (P surface doping) case (cf. Figures 3 (b) and (b')), the DOS shows that valence band maximum (VBM) exhibits a slight rise and the conduction band minimum (CBM) displays little movement, which leads to a small reduction of 0.07 eV in the band gap corresponding to band-to-band transition, in reasonable agreement with the 0.13 eV band gap narrowing of P-doped TiO_2 reported experimentally [16]. Moreover, the PDOS shows that most of the P 3p impurity states locate above the VBM and some of them lie below the CBM. It should be noted that the Fermi level E_F is pinned to the conduction band. Hence, electrons excited from the P 3p gap states to states above E_F are reduced by about 0.30 eV with respect to perfect rutile (110) surfaces, leading to an obvious red-shift of the optical absorption edge. This corresponds to gap states in the band transition, which is different from the experimental finding that visible light absorption originates from electron transition from the valence to conduction band [16]. Since the probability of transition from gap states to band states is low because the surface state involved are localized, it may be speculated that surface photovolatage spectroscopy (SPS) may measure this kind of transition through the introduction of an appropriate external electric field to magnify the SPS signal. On the other hand, the O_{ss}–doped system (cf. Figures 3 (c) and 3(c')) shows a significant difference in electronic structure with respect to the O_s case, in which the VBM displays no shift and the CBM raises by about 0.14 eV, resulting in a corresponding band gap enlargement. It is possible that this is responsible for the 0.07 eV band gap expansion reported by Yu et al. in P-doped TiO_2 [17]. However, Figure 3 (c') shows that the most of P 3p states lie in the band

gap, which results in reduction of approximately 0.77 eV in electron transition energy from P 3p gap states to the conduction band. However, this observation has not been been reported in P-doped TiO_2 in experiment to date, to the best of our knowledge.

For P-cation doping, the DOS shows opposing behavior in band gap modification for Ti_{5c} and Ti_{6c}–doped systems: the band gap is reduced for Ti_{5c}–doping, while enlarged with for the Ti_{6c} case. For the Ti_{5c}–doped system (cf. Figures 4 (b) and (b')), the DOS shows that P impurity levels have no contribution to the valence band edge and contribute partially to the conduction band edge, which leads to a narrowing of the band gap by about 0.26 eV. This is in accord the 0.22 eV decrease in band gap for P-cation doped TiO_2 reported by Lin et al. [14]. For the Ti_{6c} case (cf. Figures 4 (c) and 4(c')), however, the DOS exhibits band gap enlargement by about 0.11 eV, which approximates the 0.07 eV increase reported experimentally in P-doped TiO_2 [17]. To the best of our knowledge, this is the first time that P-cation doped TiO_2 can lead to band gap alteration has been confirmed theoretically, and P-cation doping can change the band gap in different directions, depending on doping sites.

B. P Adsorption on Rutile TiO_2 (110) Surface

For P adsorption at rutile TiO_2 (110) surfaces, there are six non-equivalent adsorption sites, namely, Top-O_b, Top-O_s, Top-Ti_{5c}, Top-Ti_{6c}, Cave, and Hollow. Table 3 (the left panel) summarizes the adsorption energies of P on different positions on the stoichiometric rutile TiO_2 (110) surface. According to Table 3, the stability of the systems is in the order: Top-Ti_{6c} > Hollow > Cave > Top-O_b > Top-O_s > Top-Ti_{5c}. The

Top-Ti_{6c} case is the most stable system with a value of 8.58 eV and the Top-Ti_{5c} is the least stable system with an adsorption energy of 12.74 eV on the rutile (110) surface. Hence, we will discuss the electronic structures of Top-Ti_{6c} model. The total electron density is presented in Figure 2(e), which shows the formation of two strong P-O **(1.558 Å)** bonds between P and adjacent to two surface bridging O atoms. On the other hand, the bond between the P atom and the sixfold coordinated Ti atom (Ti_{6c}) is weak **(i.e., a P-Ti bond length of 2.782 Å)**. This suggests that P is in a cationic state. The Bader charge on the P dopant supports the viewpoint further, whose value is 3.73 e. The DOS shows that the CBM exhibits no shift while the top of the valence band moves to a high energy region, leading to an increase in the band gap by about 0.06 eV with the respect to the perfect surface (cf. Figure 5 (b) and 5 (b')), in a very similar way to the Ti_{6c}-doped system. However, in this case, only P 3p states contribute to the bottom of the conduction band, while P 3s states have no contribution. Although the P 3s - P 3p hybrized states contribute mainly to the valence band, they have no contribution to the valence band edge and cannot serve to enhance the absorption of visible light. Further, the increase of 0.06 eV is in excellent agreement with the 0.07 eV reported experimentally [16].

3.2 Interaction between P and Surface Oxygen Vacancies on Rutile TiO_2 (110) Surface

The reactivity of the rutile TiO_2 (110) surface is highly influenced by oxygen vacancies. Furthermore, the most frequently occurring vacancies correspond to

surface bridging oxygen atoms. In this section, our main aim is to investigate whether the bridging oxygen vacancy serves to promote or hinder P substitution and adsorption. Therefore, we have calculated the formation and adsorption energies for P anion- and cation- doping on nonstoichiometric rutile TiO_2 (110) surfaces. Moreover, we have analyzed the influence of interaction between P impurities and oxygen vacancies on the electronic properties of P-doped systems based on these thermodynamic considerations.

A. Substitutional and Adsorptive P Doping on Reduced Rutile TiO_2 (110) Surface

It should be noted that reduced surface corresponds to O-poor conditions due to an oxygen deficiency. Therefore, we have calculated the formation and adsorption energies under O-poor condition only. Tables 2 and 3 (right panels) summarize the calculated formation and adsorption energies, respectively. The stability of the substituted systems is in the order: (1) for P anion doping, $O_s > O_b > O_{sb2} > O_{sb} > O_{ss}$; (2) for P cation doping, $Ti_{6c} > Ti_{s6c} > Ti_{s6c2} > Ti_{5c}$. This indicates that the most stable configurations are the O_s and Ti_{6c}-doped systems for P anion and cation doping, respectively, in the presence of surface oxygen vacancies. However, the O_{ss}- and Ti_{5c}–doped systems become the most unstable configurations with large formation energies. Furthermore, the formation energies are a bit smaller than those of oxidized surfaces expect for P occupation of the O_{sb} and Ti_{s6c} sites, indicating that incorporation of P helps to promote the formation of oxygen vacancies. Conversely, the formation of oxygen vacancies favors the implantation of P. For P adsorptive

doping, the stability is in the order: Top-Ti_{6c} > Top-O_s > Hollow > Cave > Top-O_b > Top-Ti_{5c}. The most stable configuration is still the Top-Ti_{6c}–adsorbed system with an adsorption energy of 9.33 eV, which is 0.75 eV higher than that of Top-Ti_{6c} model in the absence of surface oxygen vacancies. Further, the absorption energies of most of the systems are high in the presence of oxygen vacancies with respect to the perfect surface. Thus, P adsorption on rutile (110) surfaces is difficult in the presence of oxygen vacancies. Based on the analysis of adsorption energies, we discuss the **geometrical parameters and** electronic properties of O_s- and Ti_{6c}-substituted and Top-Ti_{6c}-adsorbed systems in detail.

In the O_s-substituted configuration, two P-Ti bonds were 2.462 Å in length, while the third one was 3.212 Å; the former two were slightly elongated and the third one was similar to the undoped case, indicating further local structure distortion. For the Ti_{6c}-substituted configuration, the optimized P-O bond lengths were 1.564, 1.701, and 2.035 Å, respectively; the former two bonds contracted (vis-à-vis 1.682 and 1.706 Å, respectively, for the perfect surface) and the latter bond became elongated (relative to the undoped case of 1.970 Å). This led to large local structure modifications. For the Top-Ti_{6c}-adsorbed case, the P-O bond was 1.626 Å in length and the P-Ti bond 2.442 Å, corresponding to a respective increase of 0.068 Å and decreases of 0.34 Å with respect to their values on a perfect surface. This indicates that the removal of one oxygen atom weakens the strength of the P-O bond and strengthens the interaction between the P and Ti atoms.

The Bader charge [35, 36] on the P impurity atom in O_s, Ti_{6c}, and Top-Ti_{6c} systems is -1.33 e, 3.39e, and 0.55 e, respectively. It indicates that the substitution of Ti by P and P adsorption on the Ti_{6c} site correspond to cation doping and the replacement of O by P is anion doping. To investigate this further, we have plotted the charge density maps in Figures 2 (f)-(h) (bottom panel). Similar to the analysis in part of 3.1, Figures 2(f), (g), (h) indicate also that a P dopant would be in anionic, cationic, and anionic states, respectively. Therefore, P may be doped into the TiO_2 lattice as either an anion or cation, depending on experimental conditions [14-17].

B. Electronic Structure of Substitutional and Adsorptive P-Doping on Reduced Rutile TiO_2 (110) Surface

To investigate the interaction between the P impurity and the bridging oxygen vacancy on the electronic structures and photocatalytic activity of P-doped TiO_2, the DOS and PDOS of O_s- and Ti_{6c}–substituted and Top-Ti_{6c}–adsorbed models were calculated and are shown in Figure 6. For comparison, the DOS and PDOS of pure rutile TiO_2 (110) surface are also shown. Before analysis of the electronic properties, one should be noted that the removal of a surface oxygen atom leads to a decrease in the number of electrons in the systems and raises the Fermi level E_F. Figure 6 shows a significant difference in electronic structures between the three doping cases but the E_F are all pinned in the conduction band. For the O_s (P- anion substituted) case (cf. Figures 6 (b) and (b')), the DOS shows an increase in the VBM of about 0.1 eV, but the CBM has also moved to a high energy region, leading to band gap enlargement.

Therefore, electronic transitions from the valence to the conduction should require larger energy. Conversely, most of the P 3p states locate within the band gap. The electronic transition energy would be reduced significantly from the P 3p states near the conduction band to the states above the E_F. The maximum reduction is about 0.8 eV compared to the perfect surface. For the Ti_{6c} (P-cation substituted) case (cf. Figures 6(c) and 6(c')), there exists an obvious difference compared with single P substitution for the six coordinated Ti atom (cf. Figures 4(c) and 4(c')). P 3s - P 3p hybridized states were found to lie in the band gap and electron transfer from the P impurity states to the states above the E_F will be reduced to a maximum value of around 0.51 eV, although the host band gap broadens with respect to perfect surface. This indicates that the interaction between P and the oxygen vacancy will extend to visible light wavelength and enhance the photocatalytic activity. For the Top-Ti_{6c} (P-cation adsorbed) system (cf. Figures 6 (d) and 4(d')), the DOS shows that two impurity states lie in the band gap and the Fermi level E_F is pinned to the conduction band, indicating that both of the two states are fully occupied. Therefore, electron transfer from the upper P 3p gap states to the states above E_F would require at least 0.94 eV, suggesting that the electron transition energy should be reduced by around 0.44 eV with respect to the perfect surface. These findings suggest that the interplay between P impurities and oxygen can lead to apparently obvious enhancements in the visible light absorption region and photocatalytic activity.

4. Conclusions

In this study, we have presented a comprehensive calculation of the effects of P doping on the rutile TiO_2 (110) surface using DFT method. The formation energy results indicate that the P atom occupies preferentially the fivefold coordinates of the Ti atom site under O-rich growth conditions, while instead for surface O_s site under Ti-rich conditions. Furthermore, under Ti-rich growth conditions, incorporation of P into O sites is more energetically favorable relative to substitution of P for Ti for both stoichiometric and non-stoichiometric surfaces. When P is adsorbed on rutile (110) surfaces, the most stable configuration is the above the sixfold coordinated Ti atom on the stoichiometric and non-stoichiometric surface. The calculated Bader charge and the charge density show that P may be in an either anionic or cationic state, depending on the doping site. The calculated DOS shows that single P anion doping will induce a slight narrowing of the band gap and introduce some P 3p states into the band gap of TiO_2, corresponds to either band-to-band transitions or transitions from gap states to band states. The former result was confirmed by experiment with band gap narrowing of 0.13 eV [17]. However, P-cation doping may lead either to small reductions in photon transition energy driven by the hybridized P 3s - P 3p gap states or result in a small band gap enlargement depending on the doping site, which is confirmed by experimental observations of a 0.22 eV decrease [14] and 0.07 eV increase in band gap [16]. The interplay between P impurities and oxygen vacancies should modify significantly the position of the Fermi level E_F and lead to enhancements in visible light absorption. Our conclusions explain well the experimental observations of lower photon absorption energy and higher photocatalytic activity under visible light with P

anion- and cation-doped TiO_2.

Acknowledgements

This work was supported by the foundation of Irish Research Council for Science, Engineering and Technology (IRCSET). The authors thank the Irish Centre for High End Computing for the provision of computational resources.

References

(1) Fujishim, A.; Honda, K. *Nature* **1972**, *238*, 37.

(2) Diebold, U. *Surf. Sci. Rep.* **2003**, *48*, 53.

(3) Asahi, R.; Morikawa, T.; Ohwaki, T.; Aoki, K.; Taga, Y. *Science* **2001**, *293*, 1457.

(4) Sato, S. *Chem. Phys. Lett.* **1986**, *123*, 126.

(5) Batzill, M.; Morales, E. H.; Diebold, U. *Phys. Rev. Lett.* **2006**, *96*, 026103.

(6) Tashikawa, T.; Tojo, S.; Kawai, K.; Endo, M.; Fujitsuka, M.; Ohno, T.; Nishijima, K.; Miyamoto, Z.; Majima, T. *J. Phys. Chem. B* **2004**, *108*, 19299.

(7) Barborini, E.; Conti, M A.; Kholmanov, I. N.; Miseri, P.; Podestå, A.; Milani, P.; Cepek, C.; Sakho, O.; Macovez, R.; Sancrotti, M. *Adv. Mater.* **2005**, *17*, 1842.

(8) **Ikeda, T.; Nomoto, T.; Eda, K.; Mizutani, Y.; Kato, H.; Kudo, A. Oishi H. J. Phys. Chem. C 2008, 112, 1167.**

(9) **Bechstein, R.; Kitta, M.; Schütte, J. KüHNLE, A.; Onishi, H. *J. Phys. Chem. C* 2009, 113, 3277.**

(10) Ohno, T.; Mitsui, T.; Matsumura, M. *Chem. Lett.* **2003**, *32*, 364.

(11) Ohno, T.; Akiyoshi, M.; Umebayashi, T.; Asai, K.; Mitsui, T.;Matsumura, M. *Appl. Catal., A* **2004**, *265*, 115.

(12) Yu, J. C.; Ho, W.; Yu, J.; Yip, H.; Wong, P. K.; Zhao, J. *En*V*iron. Sci. Technol.* **2005**, *39*, 1175.

(13) Umebayashi, T.; Yamaki, T.; Itoh, H.; Asai, K. *Appl. Phys. Lett.* **2002**, *81*, 454.

(14) Lin, L.; Lin, W.; Xie, J. L.; Zhu, Y. X.; Zhao, B. Y.; Xie, Y. C. Appl. Cataly. B 2007, 75, 52.

(15) Zheng, R. Y.; Lin, L.; Xie, J. L.; Zhu, Y. X.; Xie,Y. C. J. Phys. Chem. C 2008, 112, 15502.

(16) Lin, L.; Lin, W.; Zhu, Y. X.; Zhao, B. Y.; Xie, Y. C. Chem. Lett. 2005, 34, 284.

(17) Yu, J. C.; Zhang, L.; Zheng, Z.; Zhao, J. Chem. Mater. 2003, 15, 2280.

(18) Henderson, M. A. *Surf. Sci.* **1996**, *355*, 1511.

(19) Henderson, M. A.; Epling, W. S.; Pede, C. H. F.; Perkins, C. J. *J. Phys. Chem. B* **2003**, *107*, 534.

(20) Henderson, M. A. *Surf. Sci. Rep.* **2002**, *46*, 5.

(21) Bondarchuk, O.; Kim, Y.K.; White, J. M.; Kim, J.; Kay, B. D.; Dohnalek, Z. *J. Phys. Chem. C* **2007**, *111*, 11059.

(22) Kresse, G.; Hafner, J. *Phys. Rev. B* **1994**, *49*, 14251.

(23) Kresse, G.; Furtherműller, J. *Phys. Rev. B* **1996**, *54*, 11169.

(24) Perdew, J. P.; Burk, K.; Ernzerhof, M.; *Phys. Rev. Lett.* **1996**, *77*, 3865.

(25) Perdew, J. P.; Wang, Y. *Phys. Rev. B* **1992**, *45*, 13244.

(26) Monkhorst, H. J.; Pack, J. D. *Phys. Rev. B* **1976**, *13*, 5188.

(27) Thompsom, S. J.; Lewis, S. P. *Phys. Rev. B* **2006**, *73*, 073403.

(28) Burdett, J. K.; Hughbanks, T.; Miller, G. J.; Richardson, J. W. Jr.; Smith, J. V. *J. Am. Chem. Soc.* **1987**, *109*, 3639.

(29) Jin, H.; Dai. Y.; Wei, W.; Huang, B. B. *J.Phys. D: Appl. Phys.* 2008, *42*, 195411.

(30) **Bredow**, T.; Giordano, L.; Cinquini, F.; Pacchioni, G. *Phys. Rev. B* **2004**, *70*, 035419.

(31) Bondarchuk, O.; Kim,Y. K.; White, J. M.; Kim, J. B.; Kay, D.; Dohnalek, Z. *J. Phys. Chem. C* **2007**, *111*, 11059.

(32) Lindsay, R.; Wander, A.; Ernst, A.; Montanari, B.; Thornton, G.; Harrison, N. M. *Phys. Rev. Lett.* **2005**, *94*, 246102.

(33) Wall, C. G. V.; Neugebauer, J. *J. Appl. Phys.* **2004**, *95*, 3851.

(34) http://www.webelements.com/

(35) Davidson, E.R. *Methods in Computational Molecular Physics* edited by G.H.F. Diercksen

(36) Wilson, S. Vol. 113 *NATO Advanced Study Institute, Series C* (Plenum, New York, 1983), p. 95.

Table1. Calculated bond lengths (Å) in reconstructed rutile TiO_2 (110) surfaces. The corresponding labels can be found in Figure 1(a).

	exp. [**31**]	theory [**32**]	This work
Ti_A-O_1	*1.85*	*1.84*	*1.848*
Ti_A-O_6	*2.08*	*2.11*	*2.104*
Ti_D-O_3	*1.90*	*1.92*	*1.949*
Ti_D-O_8	*1.79*	*1.83*	*1.838*
Ti_F-O_6	*1.90*	*1.89*	*1.892*
Ti_F-O_{10}	*2.00*	*1.98*	*1.972*
Ti_F-O_{15}	*2.11*	*2.13*	*2.124*
Ti_H-O_8	*2.01*	*2.02*	*2.021*
Ti_H-O_{10}	*1.92*	*1.96*	*1.951*
Ti_H-O_{13}	*1.89*	*1.91*	*1.915*

Table 2. Formation energies (eV) for P doping in different positions of rutile TiO_2 (110) surface.

	Formation energies (eV)	
Positions	Stoichiometric	Nonstoichiometric
	Ti-rich (O-rich)	Ti-rich
O_b	*9.61 (14.58)*	*8.73*
O_s	*9.40 (14.37)*	*8.39*
O_{sb}	*9.83 (14.80)*	*9.89*
O_{sb2}	*10.57 (15.54)*	*9.79*
O_{ss}	*9.41 (14.38)*	*10.13*
Ti_{5c}	*12.08 (2.15)*	*13.01*
Ti_{6c}	*12.17 (2.24)*	*11.84*
Ti_{s6c}	*12.37 (2.44)*	*12.52*
Ti_{s6c2}	*12.50 (2.57)*	*12.74*

Table 3. Adsorption energies (eV) for P on different positions of rutile TiO_2 (110) surface. The corresponding labels can be found in Figure 1(b).

Positions	Adsorption energies (eV)	
	Stoichiometric	Nonstoichiometric
Cave	*10.33*	*10.57*
Hollow	*9.98*	*10.33*
Top-O_b	*10.32*	*10.71*
Top-O_s	*10.69*	*9.70*
Top-Ti_{5c}	*12.74*	*11.31*
Top-Ti_{6c}	*8.58*	*9.33*

Figure captions

Figure 1. Structure of rutile TiO_2 (110) surface. (a) Side view, (b) Top view. The non-stoichiometric surface corresponds to removal of one bridging oxygen atom (denoted by 1 in (a)). The large light and small dark spheres represent Ti and O atoms, respectively. The numbers and the block letters are used for identification purposes.

Figure 2 Total electron density. (a) O_s, (b) O_{ss}, (c) Ti_{5c}, (d) Ti_{6c}, and (e) Top-Ti_{6c} on stoichiometric rutile TiO_2 (110) surface. (f) O_s, (g) Ti_{6c}, and (h) Top-Ti_{6c} on non-stoichiometric rutile TiO_2 (110) surface.

Figure 3 (A) DOS (B) and PDOS for P doping on stoichiometric rutile TiO_2 (110) surface: (a) perfect rutile TiO_2(110) surface, (b) O_s model, and (c) O_{ss} model. The top of the valence band of the perfect rutile TiO_2 (110) surface is taken as the reference level. The dashed lines represent the Fermi level E_F.

Figure 4 (A) DOS (B) and PDOS for P doping on stoichiometric rutile TiO_2 (110) surface: (a) perfect rutile TiO_2 (110) surface, (b) Ti_{5c} model, and (c) Ti_{6c} model. The top of the valence band of the pure rutile TiO_2 (110) surface is taken as the reference level. The dashed lines represent the Fermi level E_F.

Figure 5 (A) DOS and (B) PDOS for P doping on stoichiometric rutile TiO_2 (110) surface: (a) perfect rutile TiO_2 (110) surface, and (b) Top-Ti_{6c} model. The top of

valence band of the perfect rutile TiO_2 (110) surface is taken as the reference level. The dashed lines represent the Fermi level E_F.

Figure 6 (A) DOS and (B) PDOS for P doping on nonstoichiometric rutile TiO_2 (110) surface: (a) perfect rutile TiO_2 (110) surface, (b) O_s, (c) Ti_{6c}, and (d) Top-Ti_{6c} model. The top of valence band of the perfect rutile TiO_2 (110) surface is taken as the reference level. The dashed lines represent the Fermi level E_F.

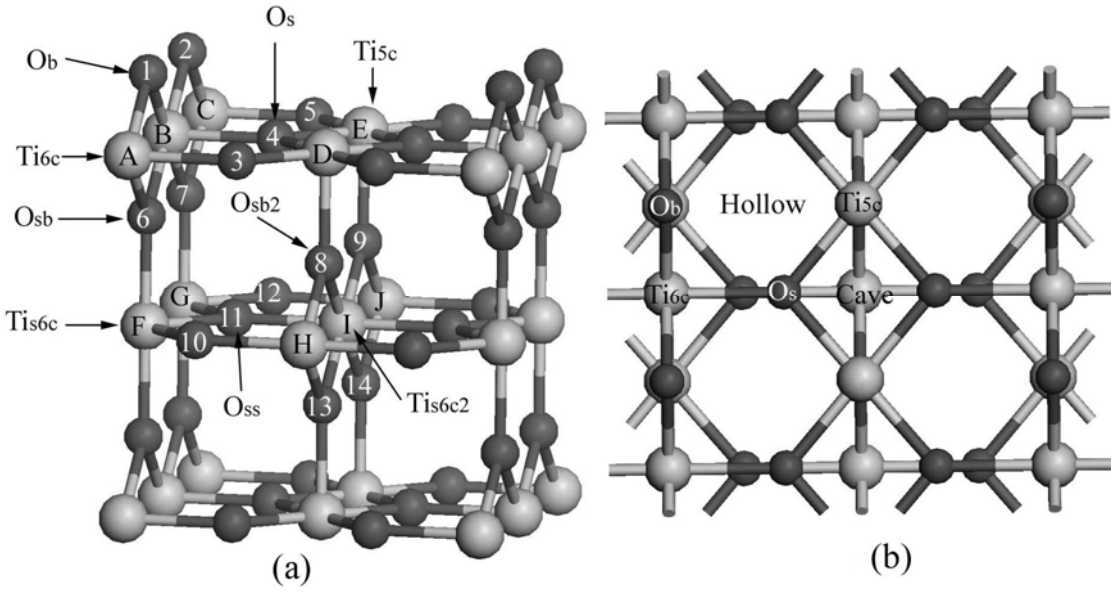

Figure 1

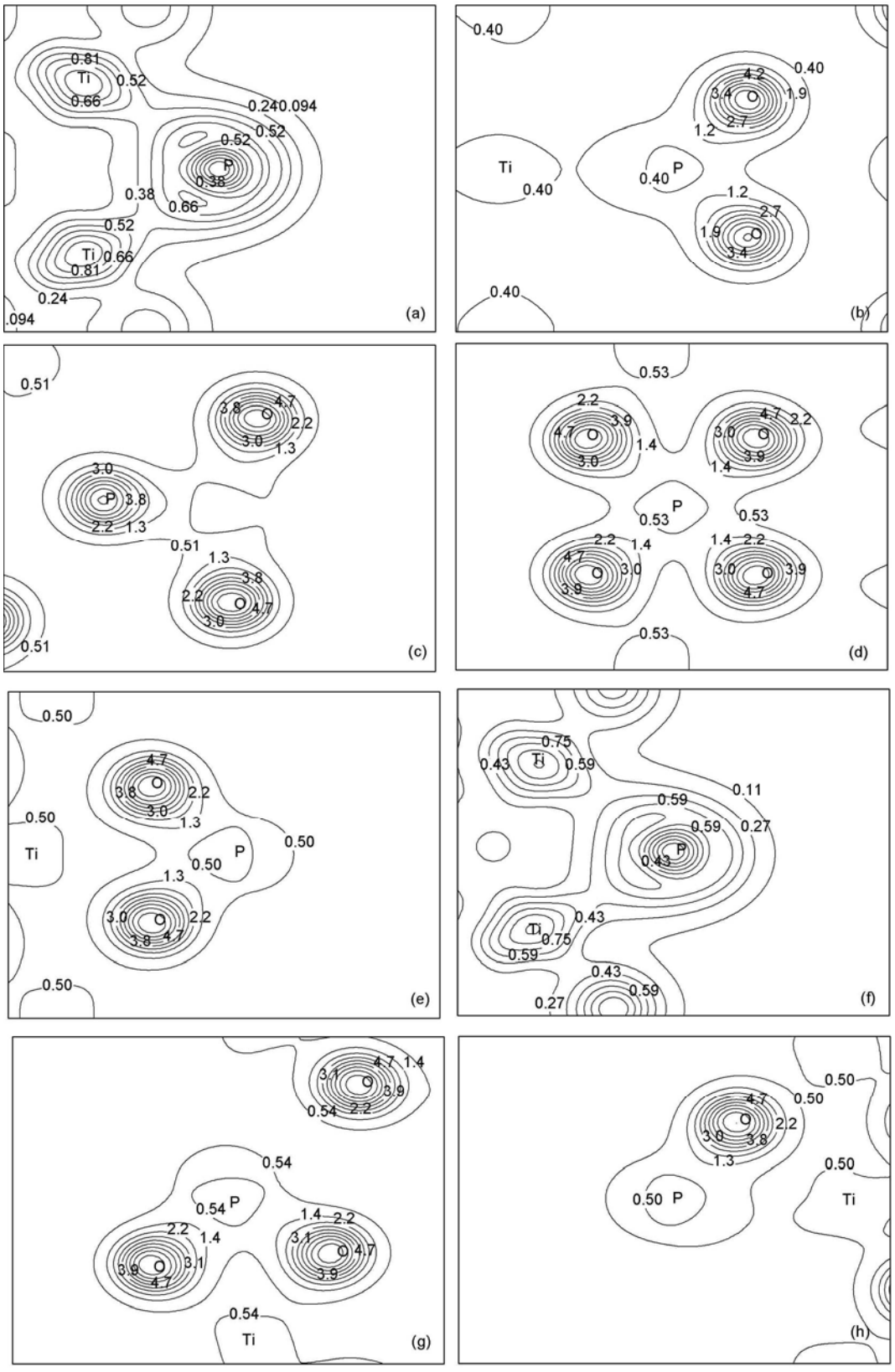

Figure 2

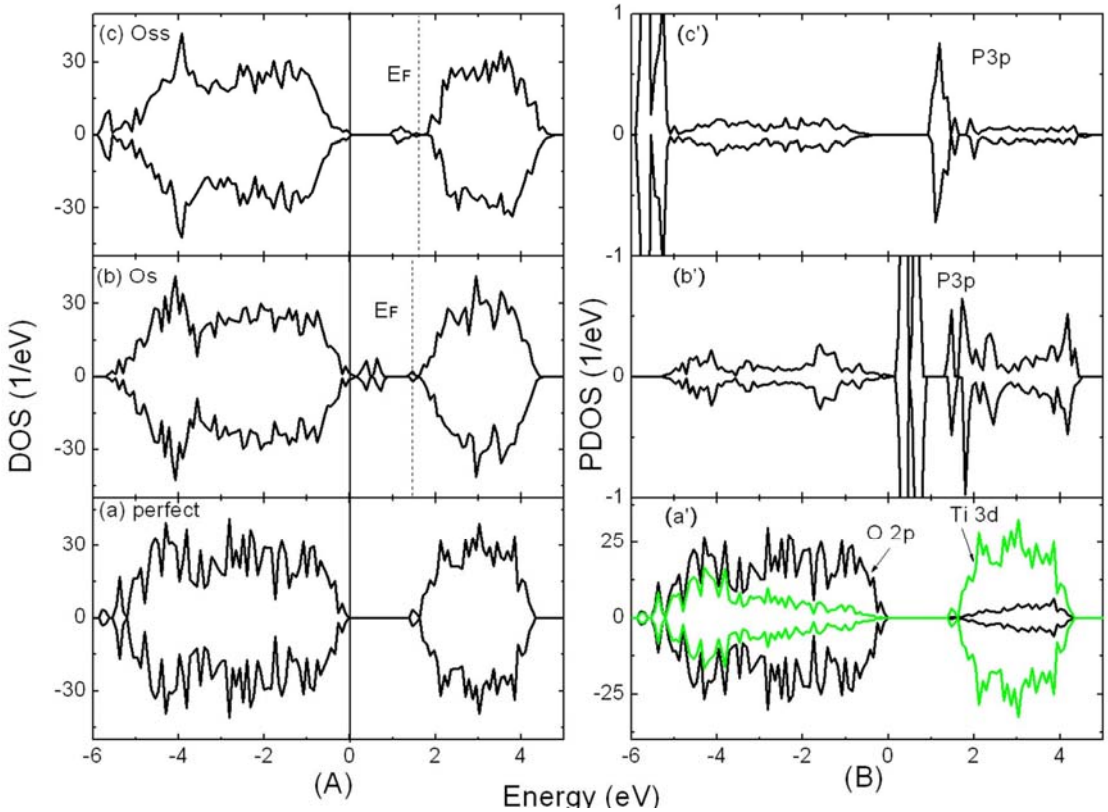
(c) Oss
(b) Os
(a) perfect
EF
EF
30
0
-30
DOS (1/eV)
(A)
(c')
P3p
(b')
P3p
(a')
O 2p
Ti 3d
1
0
-1
25
-25
PDOS (1/eV)
(B)
-6
-4
-2
0
2
4
Energy (eV)

Figure 3

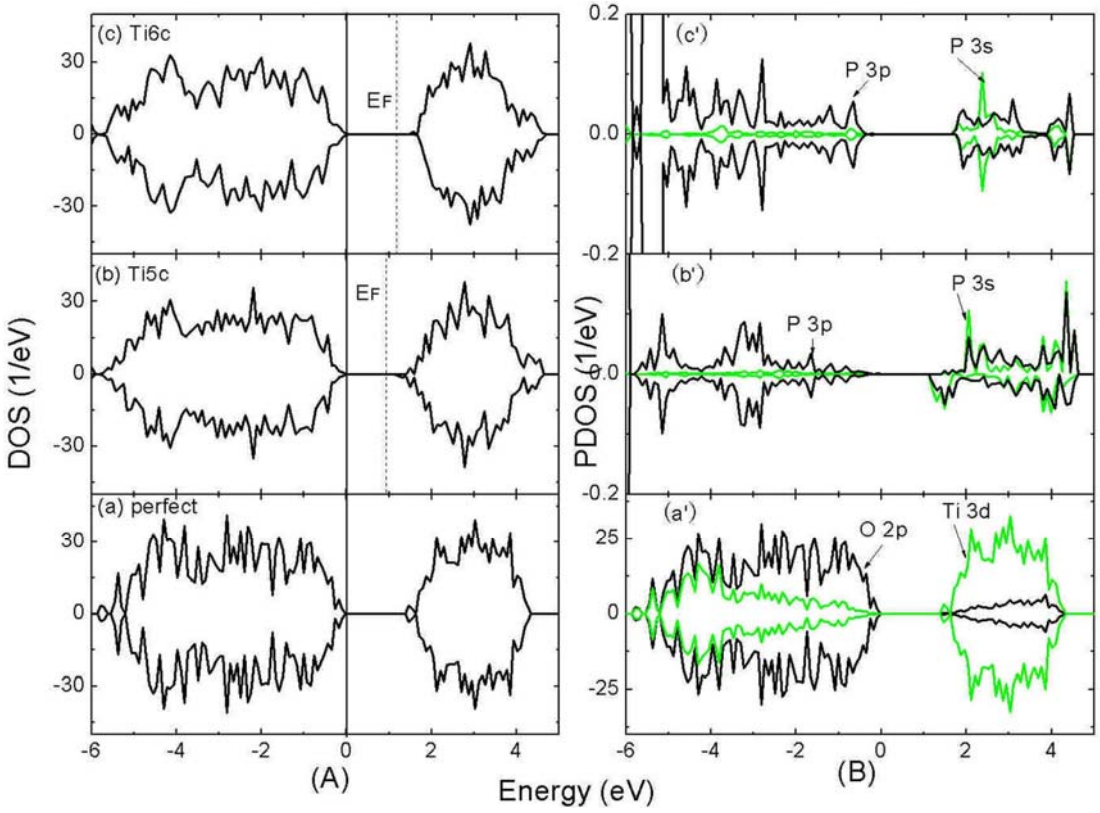
(c) Ti6c
(b) Ti5c
(a) perfect
EF
DOS (1/eV)
(A)
(c')
(b')
(a')
P 3p
P 3s
O 2p
Ti 3d
PDOS (1/eV)
(B)
Energy (eV)

Figure 4

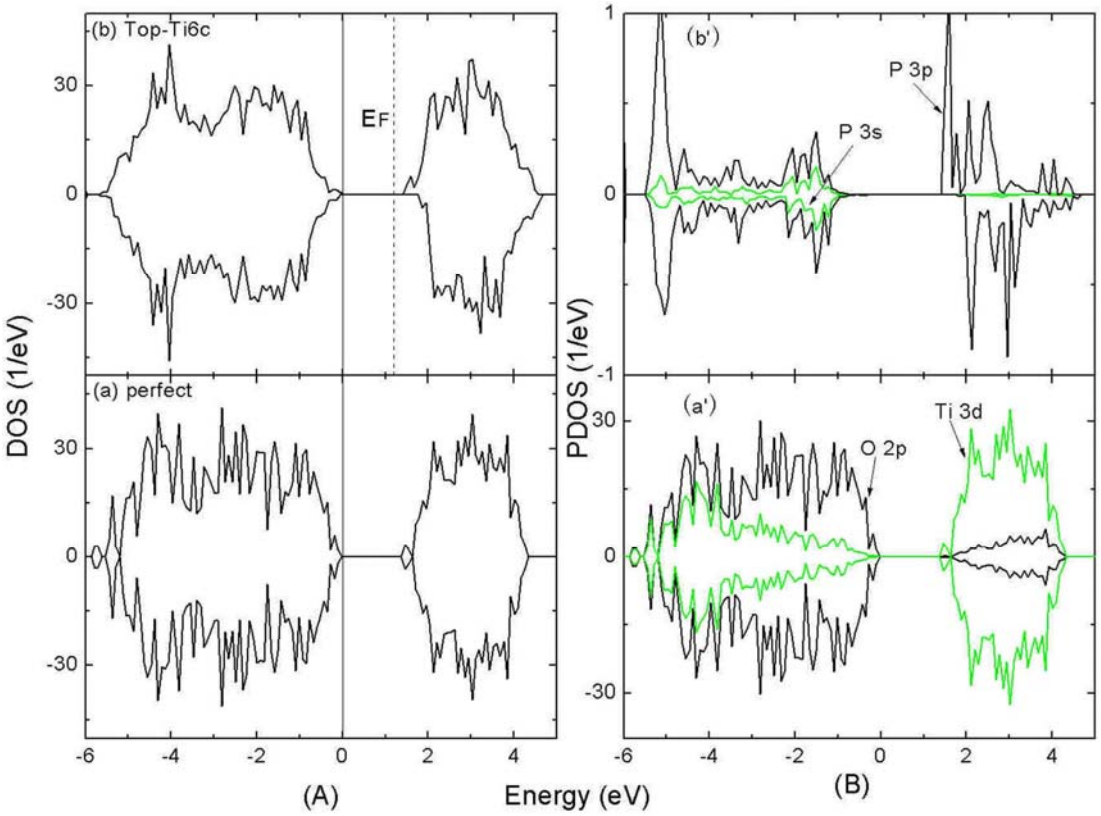
(b) Top-Ti6c
EF
(a) perfect
DOS (1/eV)
(A)
Energy (eV)
(b')
P 3p
P 3s
(a')
Ti 3d
O 2p
PDOS (1/eV)
(B)

Figure 5

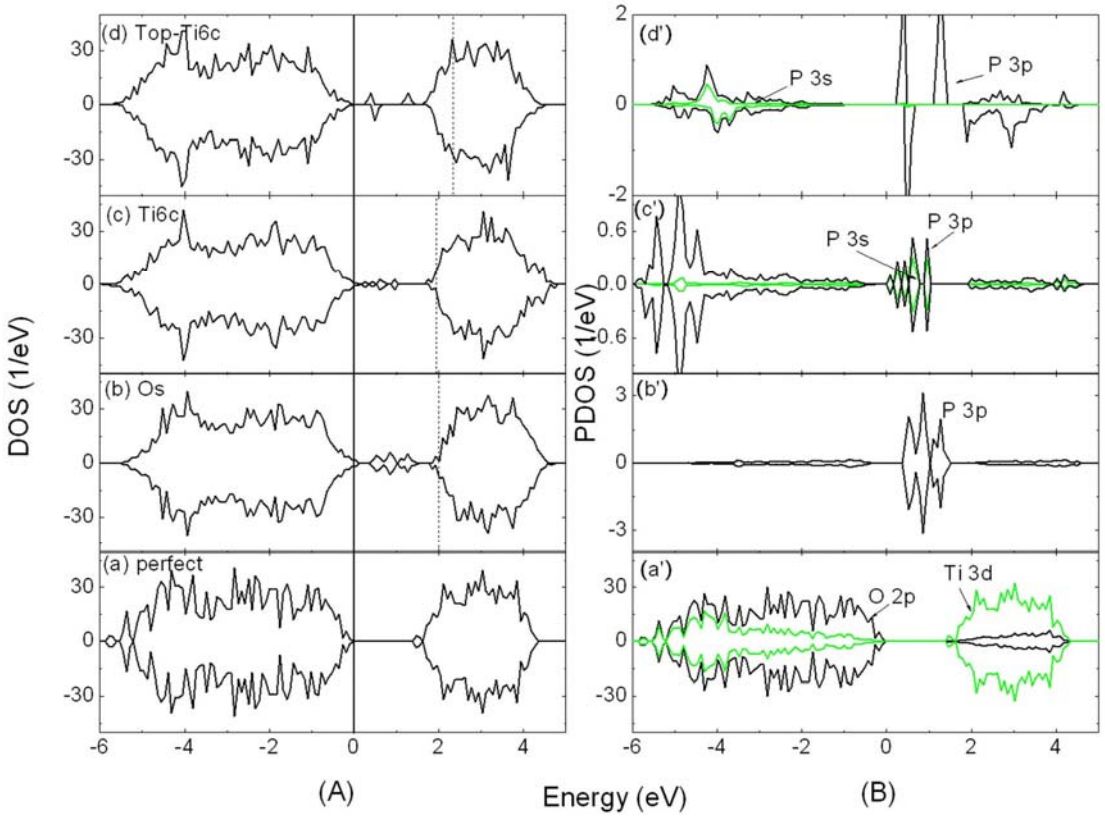
(d) Top-Ti6c
(c) Ti6c
(b) Os
(a) perfect
DOS (1/eV)
(A)
(d')
(c')
(b')
(a')
P 3s
P 3p
O 2p
Ti 3d
PDOS (1/eV)
Energy (eV)
(B)

Figure 6